AD-A040 307 POLYTECHNIC INST OF NEW YORK FARMINGDALE DEPT OF AER--ETC F/G 20/4
A TWO-LAYER MODEL FOR COUPLED THREE DIMENSIONAL VISCOUS AND INV--ETC(U)
JUN 75 S G RUBIN, T C LIN AF-AFOSR-2635-74
UNCLASSIFIED POLY-AE/AM-75-10 AFOSR-TR-77-0685 NL

| OF |
AD A040307

END

DATE FILMED
7-77

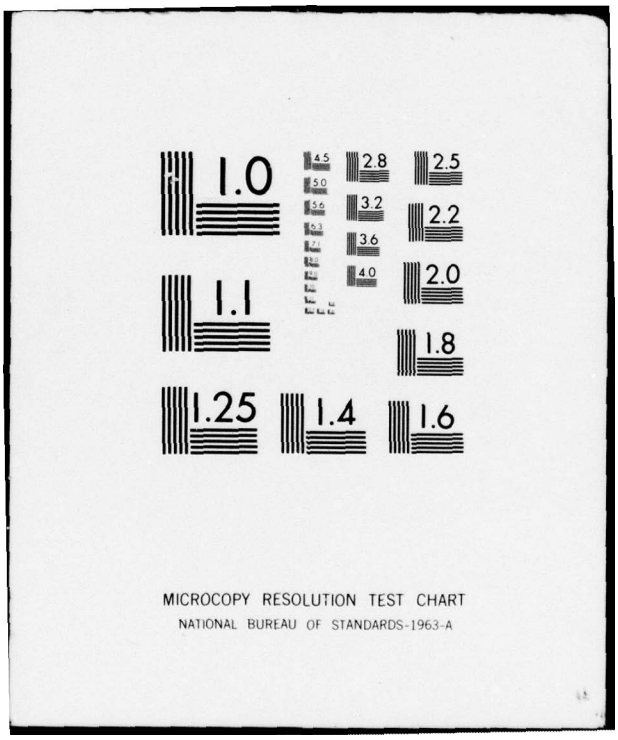
1.0
1.1
1.25
1.4
1.6
1.8
2.0
2.2
2.5
2.8
3.2
3.6
4.0
4.5
5.0
5.6
6.3
7.1
MICROCOPY RESOLUTION TEST CHART
NATIONAL BUREAU OF STANDARDS-1963-A

AD A040307

SECURITY CLASSIFICATION OF THIS PAGE (When Data Entered)

REPORT DOCUMENTATION PAGE

READ INSTRUCTIONS BEFORE COMPLETING FORM

1. REPORT NUMBER: AFOSR - TR - 77 - 0685	2. GOVT ACCESSION NO.
3. RECIPIENT'S CATALOG NUMBER	
4. TITLE (and Subtitle): A TWO-LAYER MODEL FOR COUPLED THREE DIMENSIONAL VISCOUS AND INVISCID FLOW CALCULATIONS •	5. TYPE OF REPORT & PERIOD COVERED: INTERIM rept.
6. PERFORMING ORG. REPORT NUMBER: POLY-AE/AM Report No-75-10	
7. AUTHOR(s): S. G. RUBIN, T. C. LIN	8. CONTRACT OR GRANT NUMBER(s): AF - AFOSR 74-2635-74
9. PERFORMING ORGANIZATION NAME AND ADDRESS: POLYTECHNIC INSTITUTE OF NEW YORK, ROUTE 110, FARMINGDALE, NEW YORK 11735	10. PROGRAM ELEMENT, PROJECT, TASK AREA & WORK UNIT NUMBERS: 9781-02, 61102F, 02
11. CONTROLLING OFFICE NAME AND ADDRESS: AIR FORCE OFFICE OF SCIENTIFIC RESEARCH/NA, 1400 WILSON BOULEVARD, ARLINGTON, VIRGINIA 22209	12. REPORT DATE: June 1975
	13. NUMBER OF PAGES: 19
14. MONITORING AGENCY NAME & ADDRESS (if different from Controlling Office): 21p. AFOSR TR-77-0685	15. SECURITY CLASS. (of this report): UNCLASSIFIED
	15a. DECLASSIFICATION/DOWNGRADING SCHEDULE

16. DISTRIBUTION STATEMENT (of this Report)

Approved for public release; distribution unlimited.

DDC RELEASED JUN 8 1977 C

17. DISTRIBUTION STATEMENT (of the abstract entered in Block 20, if different from Report)

18. SUPPLEMENTARY NOTES

PROCEEDINGS
AIAA Fluid and Plasma Dynamics Conference 8th Hartford, Connecticut
16-18 June 1975

19. KEY WORDS (Continue on reverse side if necessary and identify by block number)

BOUNDARY LAYER/BOUNDARY REGION
INVISCID FLOW
LAMINAR
TURBULENT
BLUNT BODY

20. ABSTRACT (Continue on reverse side if necessary and identify by block number)

A numerical finite difference method is developed to simulate the viscous flow over blunt/sharp bodies at incidence. Herein, a two-layer model is suggested. The inner region consists of the three-dimensional boundary layer and boundary region. Laminar and turbulent flows are considered. The governing system applies in boundary regions and for problems with cross flow reversal. The equations are integrated by a predictor-corrector scheme. For the turbulent boundary layer analysis, both a mixing length model and a two-equation kinetic energy-dissipation system is considered for Reynolds stress closure. The outer

next page LB

DD FORM 1 JAN 73 1473 EDITION OF 1 NOV 65 IS OBSOLETE

UNCLASSIFIED

SECURITY CLASSIFICATION OF THIS PAGE (When Data Entered)

region is inviscid. The Euler equations are integrated with McCormack's two level explicit scheme. For the matching of the two regions, three dimensional viscous displacement and entropy layer swallowing are considered. Numerical solutions are compared with experimental data and indicate that the present formulation can give an accurate prediction of aerodynamic loads, skin friction and heat transfer rates on sphere-cone-cylinder-flare shape bodies at angle of attack. The calculations are suitable for (i) supersonic or hypersonic freestreams, (ii) large Reynolds number and (iii) flows without streamwise flow separation; however, secondary flow reversal is allowed.

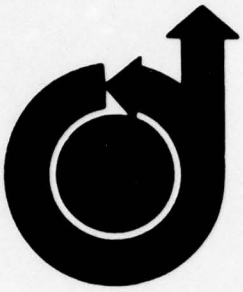

AIAA PAPER No. 75-853

A TWO-LAYER MODEL FOR COUPLED THREE DIMENSIONAL VISCOUS AND INVISCID FLOW CALCULATIONS

by
T. C. LIN
Avco Systems Division
Wilmington, Massachusetts
and
S. G. RUBIN
Polytechnic Institute of New York
Farmingdale, New York

AIAA 8th Fluid and Plasma Dynamics Conference

HARTFORD, CONNECTICUT/JUNE 16-18, 1975

A TWO-LAYER MODEL FOR THREE DIMENSIONAL VISCOUS AND INVISCID FLOW CALCULATIONS*

T. C. Lin
Avco Systems Division
Wilmington, Massachusetts

and

S. G. Rubin
Polytechnic Institute of New York
Farmingdale, New York

Abstract

A numerical finite difference method is developed to simulate the viscous flow over blunt/sharp bodies at incidence. Herein, a two-layer model is suggested. The inner region consists of the three-dimensional boundary layer and boundary region. Laminar and turbulent flows are considered. The governing system applies in boundary regions and for problems with cross flow reversal. The equations are integrated by a predictor-corrector scheme. For the turbulent boundary layer analysis, both a mixing length model and a two-equation kinetic energy-dissipation system is considered for Reynolds stress closure. The outer region is inviscid. The Euler equations are integrated with McCormack's two level explicit scheme. For the matching of the two regions, three dimensional viscous displacement and entropy layer swallowing are considered. Numerical solutions are compared with experimental data and indicate that the present formulation can give an accurate prediction of aerodynamic loads, skin friction and heat transfer rates on sphere-cone-cylinder-flare shape bodies at angle of attack. The calculations are suitable for (i) supersonic or hypersonic freestreams, (ii) large Reynolds number and (iii) flows without streamwise flow separation; however, secondary flow reversal is allowed.

Nomenclature

a, b, k	constants defined in eq. (24)
a_1, b_2, b_1	constants defined in eq. (14)
$A^+ = 26\sqrt{\rho_w/\rho}\ \mu/\mu_w$	
$d = \delta - \Delta$	
E, F, G, I	Matrices defined in eq. (1)
$F = U/U_e$	
$G = W/W_e$	
h	constant defined in eq. (13) or local enthalpy
h_ξ, h_ϕ	metric coefficients defined in eq. (11a)
H	total enthalpy
K	turbulence kinetic energy
L	characteristic length
M	Mach number
p	pressure
Pr	Prandtl number
$q = (u^2 + w^2)^{1/2}$	
$\dot{q}$	surface heat transfer
$\dot{q}_{cw} = \dot{q}/\left[Tr/To - Tw/To\right]$	
$Re_\theta = \rho_e U_e \theta/\mu_e$	
s	surface length
$t = \int_0^\xi \rho_e \mu_e U_e h \phi^2 h_\xi \, d\xi$	
T	static temperature
u, v, w	velocity components
x, y, z	coordinate frame
α	angle of attack
β	variable defined in eq. (6)
$\gamma = C_p/C_v$	
Δ	three dimensional viscous displacement thickness
δ	boundary layer thickness
$\delta_x^* = \int_0^\delta \left(1 - \frac{\rho u}{\rho_e U_e}\right) dy$	

*This research is jointly sponsored by the Air Force office of Scientific Research (under Grant No. AFOSR 74-2635) and the Avco Independent Research and Development program.

$\delta_\phi^* = \int_0^\delta \left(1 - \rho w / \rho_e w_e\right) d y$

θ local body slope

$\Lambda = \rho_e \mu_e U_e h_\phi^2 h_\xi$

Λ_1 variable defined in eq. (24)

μ_t turbulent Eddy viscosity

μ_e molecular viscosity

ξ, η, ϕ coordinate frame

τ_w shear stress at the wall

ρ density

ϵ turbulence dissipation function

λ constant defined in eq. (17)

subscripts

s refers to shock

b, w refers to surface condition

e refers to boundary layer edge conditions

ϕ, ξ indicates $\partial(\,)/\partial\phi$, $\partial(\,)/\partial\xi$ respectively

∞ refers to free stream conditions

I. Introduction

During the last decade, numerical computations for both boundary layers[1-3] and inviscid flows[4-7] have been advanced considerably in capability, speed and accuracy. However, the computational procedures for these two flow regions have been primarily developed independently so that the effects of viscous-inviscid interactions have been largely neglected.

In many cases an inviscid calculation may become inaccurate unless proper consideration is given to the surface viscous interaction. On the other hand, accurate boundary layer edge properties are sometimes difficult to obtain unless a meaningful inviscid computational program is available. Therefore, numerical calculations of the inner (viscous) and outer (inviscid) regions should be properly interrelated by suitable matching conditions. While this has been done for two dimensional flows, three dimensional matched solutions for general geometries have not been previously obtained.

Direct integration of the complete Navier-Stokes equations avoids the matching process. This has been carried out successfully by a number of researchers for laminar[8] and more recently turbulent flow.[9] However, these efforts are still largely confined to either two dimensional or axisymmetric geometries and even then are quite time consuming. A second approach uses a simplified Navier-Stokes system. Its salient feature is a single-layer model[10-13] that also precludes the necessity for matching of the inner and outer regions. Although this approach has been successful in a number of problems, the computation times can become excessive. One inherent difficulty in the single layer model is the specification of one coordinate system to account for the two different length scales in the viscous and inviscid regions. For example the laminar boundary layer thickness may increase as $\sqrt{x}$ (x - streamwise distance), while the outer bow shock grows linearly. It is difficult for a single coordinate transformation to take into consideration the different growth rates associated with these two distinct regions. Therefore, the two-layer model proposed here appears to be a practical and economical alternative for weak interaction three-dimensional flow calculations.

The formulation, governing equations and numerical methods for the inner (viscous) and outer (inviscid) regions will be briefly discussed in sections II and III. Typical numerical solutions are compared with existing experimental data. The inner and outer solutions are then coupled by including the pertinent effects of viscous displacement and entropy layer swallowing effects. This procedure is described in section IV where some relevant examples are depicted.

II. Outer Inviscid Flow

The three dimensional inviscid flow in the shock layer of a blunt non-circular body at angle of attack is considered. A time dependent finite-difference technique is applied for the subsonic nose region and streamwise marching procedure for the supersonic afterbody. A two-level explicit scheme is used for the calculation of the internal points and a modified method of characteristics procedure is applied at boundary and shock points.

II.1 Supersonic Region

The inviscid formulation is patterned after that of Moretti;[14, 15] however, the governing equations are written in divergence form. The Euler equations in cylindrical coordinate are:

$$E_\xi + F_\eta + G_\phi + I = 0 \qquad (1)$$

where $E = \begin{vmatrix} \rho u \\ \rho u^2 + p/M_\infty^2 \gamma \\ \rho u v \\ \rho u w \end{vmatrix}$

$G = \begin{vmatrix} \rho w r^{-1} \\ \rho u w r^{-1} \\ \rho v w r^{-1} \\ \left(\rho w^2 + p/M_\infty^2 \gamma\right) r^{-1} \end{vmatrix}$

$F = E\eta_z + G\eta_\phi + \begin{vmatrix} \rho v \\ \rho u v \\ p/M_\infty^2 \gamma + \rho v^2 \\ \rho v w \end{vmatrix}$

$I = \begin{vmatrix} \rho v r^{-1} \\ \rho u v r^{-1} \\ \rho(v^2 - w^2) r^{-1} \\ \rho v w \end{vmatrix} + A_1 E + A_2 G$

$A_1 = \left[(r_s)_z - (r_b)_z\right] \Big/ \left[r_s - r_b\right]$

$A_2 = \left[(r_s)_\phi - (r_b)_\phi\right] \Big/ \left[r_s - r_b\right]$

$\eta = (r - r_b) \Big/ (r_s - r_b)$

Here u, v, w, p and ρ are nondimensionalized with respect to free stream flow properties. The temperature distribution is evaluated from the following isoenergtic conditon,

$$T = p/\rho = 1 + \frac{\gamma-1}{2} M_\infty^2 - \frac{1}{2} M_\infty^2 (\gamma-1)(u^2+v^2+w^2) \tag{2}$$

An explicit numerical method is employed. The two level integration scheme suggested by McCormack[16] has been adopted for the interior points. The marching Δz is limited by the Courant-Frederick-Levy conditon.

The outer bow shock, $r_s = r_s(z, \phi)$ is treated as discontinuity. Flow properties behind the shock are evaluated from the Rankine-Hugoniot relation once the normal velocity component $\bar{U}_\infty \cdot \nabla r_s$ is obtained. An additional condition which determines the value or equivalently the shock orientation is supplied by the following characteristic compatibility relation:

$$\partial^2 r_s / \partial z^2 = f(\rho_\eta, u_\eta, v_\eta, w_\phi, u_\phi, v_\phi) \tag{3}$$

The complete expression for $\partial^2 r_s / \partial z^2$ is derived in Reference (15). Eq. (3) is valid along the right running characteristic surface defined by

$$\frac{d\eta}{dz} = \lambda$$

$$\lambda = \Delta \Big\{ Au - \frac{I}{M_\infty^2}\eta_z + \frac{I}{M_\infty^2}\sqrt{\left[\left(v\eta_r + \frac{w}{r}\eta_\phi\right)^2 + \eta_r^2\left(u^2 - \frac{I}{M_\infty^2}\right)\right]\left(\frac{I}{M_\infty^2}\right)^{-1}} \tag{4}$$

$A = u\eta_z + v\eta_r + \frac{w}{r}\eta_\phi$, $\Delta = \left(u^2 - \frac{I}{M_\infty^2}\right)^{-1}$

McCormack's scheme is also used to integrate eq. (3) for $(r_s)_z$. Here $\partial(\,)/\partial r$ is evaluated by a three-point end difference formula. It should be noted that iteration is unnecessary for the formulation on boundary points.

On the body surface, it is required that

$$\bar{q} \cdot \nabla r_b = 0 \tag{5}$$

The wall pressure is obtained from the compatibility relation along the left running characteristic, i.e.

$$\begin{aligned} p_z = {} & -\lambda p_\eta + \frac{\gamma M_\infty^2 \rho}{T\beta}\Big\{ \lambda\left|u v_\eta - \left(v - \frac{w}{r} r_{b_\phi}\right) u_\eta\right| \\ & + u^2 r_{b_{zz}} + \frac{u w_z}{r}(r_b)_\phi + \frac{u w}{r}(r_b)_{\phi z} \\ & - \frac{u w}{r_b^2}(r_b)_\phi (r_b)_z \Big\} + \frac{\gamma\Delta}{\beta r} p\left[v - \frac{w}{r} r_{b_\phi} - \beta u\right] \\ & + \left[\frac{w p_\phi}{p\gamma} + w_\phi + v + w\eta\right]\eta_\phi \\ & + \frac{p w M_\infty^2 \gamma}{T\beta r}(v_\phi - w) - \frac{w M_\infty^2 \gamma p}{T\beta r}\left|\left(v - \frac{w}{r} r_{b_\phi}\right) u - \frac{\beta T}{M_\infty^2}\right| u_\phi \end{aligned}$$

where $\lambda = \frac{d\eta}{dz} = \frac{T\eta_r \Delta}{M_\infty^2}\left|(r_b)_z - \beta\right|$

$$\beta = \sqrt{u^2\left(1 + r_{b_z}^2\right)\left(\frac{I}{M_\infty^2}\right)^{-1} - 1} \tag{6}$$

Since the body entropy is known, the density can be computed from the isentropic relation. Finally the velocity components at wall are calculated from eqs. (2) and (5).

II.2 Inviscid Blunt Body Calculation

Moretti's[4] time-dependent blunt body program has been used to calculate the flow field in the subsonic nose region. This code is more versatile than the inverse method of Ref. (7), particularly when the free stream Mach number is low ($M_\infty \leq 3$), and the body is other than the sphere-cone geometry. Recently this numerical program has been modified to include real gas and nonuniform free stream effects.[5] The blunt body solutions supply the starting conditions for the downstream supersonic flow calculations.

II.3 Results for Inviscid Flow

In order to check the computer code

and to demonstrate its capability several sample calculations are presented here. The surface pressure distribution over an elliptic cone (b/A = 1.79) at 15° angle of attack is depicted in Fig. 2. Comparison is made with Zakkay and Visich's data;[17] the agreement is encouraging. It should be noted that for $\alpha/\theta \geq 1.5$ (α = angle of attack, θ = cone half angle) the inviscid computational for a sharp cone becomes unstable and the inner viscous region cannot be neglected. The aim of our present work is to correct the deficiency of the inviscid solution by matching with the boundary layer.

Fig. 3 shows the inviscid results over a sphere cone ($\theta = 9^\circ$) at angle of incidence ($\alpha = 4^\circ$ and 10°). The expansion-recompression processes near the junction of sphere and cone are simulated quite well by the finite difference solutions.

The last case considered is the surface pressure distribution on a cone-cylinder-flare which is shown in Fig. 4. Also presented are Zakkay and Callahan's experiment measurements.[18]

In summary, it has been demonstrated that the numerical code for the inviscid flow is reasonably accurate and versatile. In the following section, the formulation for the inner region is discussed.

III. Inner Layer (Viscous Region)

Many of the existing theoretical studies of three dimensional boundary layer either assume a similarity approximation[19] (such that the governing equations become pseudo two dimensional), or resort to a small cross flow approximation[20, 21] or independence principle. The nature of the three dimensional boundary layer equations has been investigated by Der and Raetz.[22] Recently Davis[23, 24] and his associates have made a series of studies on numerical methods for nonsimilar boundary layers on sharp as well as blunt bodies. Generally the Dwyer-Krause method[25, 26] is suitable for boundary layer computations, but without the existence of boundary regions. The formulation suggested by Lin and Rubin[27-30] can handle problems with boundary regions. One advantage of this method is the ability to resolve flows with crossflow reversal. Significantly this procedure also removes the difficulty concerning existence and uniqueness of the solutions near the leeplane.[30a]

Recently, Blottner and Ellis[31] have generalized the Dwyer-Krause scheme for laminar incompressible flow, furthermore, they suggest a system of useful coordinates for blunt body calculations.

III.1 Formulation

It has been observed experimentally[52] and analytically[13, 29] that secondary flow reversal does not occur at the tip of a sharp cone, or in a blunted nose region when the body is at moderate angle of incidence. This important observation is implicit in the present theoretical formulation. Herein, the Blottner and Ellis procedure[31] will be adopted for flow in the blunt nose region, while the predictor-corrector formulation[27-30] is used for the afterbody supersonic flow. This choice is acceptable as a boundary region does not appear near the nose, but cross flow reversal is possible in the downstream flow. These two approaches were originally designed for laminar flow, but are extended to turbulent flow conditions in the present paper.

III.1.A Blunt Body Region

A body orientated coordinate system suggested by Blottner and Ellis[31] is employed here (Fig. 5). One coordinate is defined from the intersection of the body surface with the plane containing the x-axis and at an angle ϕ from the y-axis. These lines define the coordinate ϕ = constant, (here one would choose the y-axis to be the symmetry plane). The other coordinates are orthogonal ξ = constant lines, (see Fig. 5).

The surface of the body is defined by an expression of the form

$$x_1 = x_1(x_2, \phi), \qquad x_2 = x_2(x_1, \phi)$$

where x_1 and x_2 represent x and r respectively. The position vector $\bar{r}$ can be written as

$$\bar{r} = x\,\bar{i} + r\cos\phi\,\bar{j} + r\sin\phi\,\bar{k}$$

Vectors that are tangent to ϕ = constant and ξ = constant are $\bar{s} = (\partial \bar{r}/\partial \xi)_\phi$ and $\bar{t} = (\partial \bar{r}/\partial \phi)_\xi$ respectively. For the coordinates to be orthogonal, the relation $\bar{s}\cdot\bar{t} = 0$ must be satisfied. This leads to

$$\left(\frac{\partial x_2}{\partial \phi}\right)_\xi = \lambda = -\frac{\left(\frac{\partial x_1}{\partial x_2}\right)_\phi \left(\frac{\partial x_1}{\partial \phi}\right)_{x_2}}{1 + \left(\frac{\partial x_1}{\partial x_2}\right)^2_\phi} \tag{7}$$

Along ξ = constant, this relation is written in finite-difference form as

$$(x_2)_{K+1} = (x_2)_K + \lambda_{K+\frac{1}{2}} \Delta\phi \tag{8}$$

For points along the symmetry line, we obtain:

$$\Delta x_2 = \Delta S \Big/ \sqrt{1 + \left(\partial x_1/\partial x_2\right)^2} \tag{9}$$

$$\Delta S = h_\xi\, d\xi \quad \text{along} \quad \phi = 0$$

The metric coefficients are found from the definition:

$$h_\xi = \left(dx^2 + dr^2\right)^{1/2} \Big/ d\xi$$

$$h_\phi = \left[dx^2 + dr^2 + (r\,d\phi)^2\right] \Big/ d\phi \qquad (10)$$

Eqs. (10) are expressed in finite difference form in the numerical computations.

If the inviscid flow on the body surface is given in terms of the (x, y, z) coordinates (Fig. 5), so that

$$\bar{u}_T = u_1\,\bar{i} + v_1\,\bar{j} + w_1\,\bar{k}$$

then the velocity components parallel to the ξ and ϕ planes can be found from

$$u_e = \left(\bar{u}_T \cdot \bar{s}\right)/|\bar{s}|$$

$$w_e = \left(\bar{u}_T \cdot \bar{t}\right)/|\bar{t}|$$

The three dimensional boundary layer equations in terms of the curvilinear coordinates (ξ, η, ϕ) can be written as:

continuity

$$(V_2)_\eta + \frac{\sqrt{2t}}{\Lambda}\left[\frac{\partial}{\partial\xi} F\sqrt{2t} + \frac{\partial}{\partial\phi} W \frac{h_\xi}{h_\phi}\sqrt{2t}\right] = 0$$

ξ momentum

$$V_2 F_\eta + \frac{2t}{\Lambda}\left\{FF_\xi + W\frac{h_\xi}{h_\phi}F_\phi + \left(F^2 - \textcircled{H}\right)\frac{\partial \ln u_e}{\partial\xi} + \left(WF - w_e\textcircled{H}\right)\left[\frac{h_\xi}{h_\phi}\frac{\partial \ln u_e}{\partial\phi} + \frac{1}{h_\phi}\frac{\partial h_\xi}{\partial\phi}\right] - \frac{\partial \ln h_\phi}{\partial\xi}\left(W^2 - w_e^2\textcircled{H}\right)\right\} = \frac{\partial}{\partial\eta}\left(\tilde{\rho}\tilde{\mu}F_\eta\right)$$

ϕ momentum

$$V_2 W_\eta + \frac{2t}{\Lambda}\left\{FW_\xi - \textcircled{H}w_{e\xi} + \left(FW - w_e\textcircled{H}\right)\left[\frac{\partial \ln u_e}{\partial\xi} + \frac{\partial \ln h_\phi}{\partial\xi}\right] = -\frac{1}{h_\phi}\frac{\partial h_\xi}{\partial\phi}\left(F^2 - \textcircled{H}\right) + \left(W^2 - W^2\textcircled{H}\right)\frac{h_\xi}{h_\phi}\frac{\partial \ln u_e}{\partial\phi}\right.$$

$$\left. + \frac{h_\xi}{h_\phi}\left[W\frac{\partial W}{\partial\phi} - w_e\textcircled{H}\frac{\partial w_e}{\partial\phi}\right] = \frac{\partial}{\partial\eta}\left[\tilde{\rho}\tilde{\mu}\frac{\partial W}{\partial\eta}\right]\right. \qquad (11)$$

energy

$$V_2\textcircled{H}_\eta + \frac{2t}{\Lambda}\left[F\textcircled{H}_\xi + W\frac{h_\xi}{h_\phi}\textcircled{H}_\phi\right] = \tilde{\rho}\tilde{\mu}M_e^2(\gamma-1)\left(F_\eta^2 + W_\eta^2\right) + \frac{1}{Pr}\frac{\partial}{\partial\eta}\left(\tilde{\rho}\tilde{\mu}\textcircled{H}_\eta\right) + \frac{2t}{\Lambda}\textcircled{H}\left(F - W\frac{u_e}{w_e}\right)$$

$$\left\{\frac{\gamma-1}{\gamma}\frac{\partial \ln P}{\partial\xi} + \left(\frac{u_\infty}{u_e}\right)^2 M_e^2(\gamma-1)\left[\frac{u_e}{u_\infty}\left(\frac{u_e}{u_\infty}\right)_\xi + \left(\frac{w_e}{u_\infty}\right)\left(\frac{w_e}{u_\infty}\right)_\xi\right]\right\}$$

where

$$F = \bar{u}/\bar{u}_e\,,\quad W = \bar{w}/\bar{u}_e\,,\quad \textcircled{H} = \bar{T}/\bar{T}_e$$

$$\tilde{\rho} = \bar{\rho}/\bar{\rho}_e\,,\quad \tilde{\mu} = \bar{\mu}/\bar{\mu}_e\,,\quad M_e = u_e/a_e$$

$$V_2 = \frac{\sqrt{2t}}{\Lambda}\left[\bar{\rho}\,\bar{v}\,h_\xi h_\phi + \sqrt{2t}\,F\eta_\xi + W\sqrt{2t}\,\frac{h_\xi}{h_\phi}\eta_\phi\right]$$

$$\eta = \frac{u_e h_\phi}{\sqrt{2t}}\int_0^\eta \rho\,d\eta\,,\quad \bar{t} = \int_0^\xi \bar{\rho}_e\bar{\mu}_e\bar{u}_e\bar{h}_\phi^2\bar{h}_\xi\,d\xi$$

$$\Lambda = \frac{\partial \bar{t}}{\partial\xi}\,,\quad h_\xi = \bar{h}_\xi/L\,,\quad h_\phi = \bar{h}_\phi/L$$

The metric coefficients h_ξ and h_ϕ which were given in eq. (10) are defined as

$$ds^2 = h_\xi^2\,d\xi^2 + h_\phi^2\,d\phi^2 + d\eta^2 \qquad (11a)$$

Along the symmetric line these equations can be simplified to:

continuity

$$(V_2)_\eta + \frac{\sqrt{2t}}{\Lambda}\left[\frac{\partial}{\partial\xi}F\sqrt{2t} + \frac{1}{u_e}\frac{\partial w_e}{\partial\phi}\frac{h_\xi}{h_\phi}\sqrt{2t}G\right] = 0$$

ξ momentum

$$V_2 F_\eta + \frac{2t}{\Lambda}\left[FF_\xi + \left(F^2 - \textcircled{H}\right)\frac{\partial \ln u_e}{\partial\xi}\right] = \frac{\partial}{\partial\eta}\left(\tilde{\rho}\tilde{\mu}F_\eta\right)$$

ϕ momentum

$$V_2 G_\eta + \frac{2t}{\Lambda}\left\{FG_\xi + \left(FG - \textcircled{H}\right)\left[\frac{\partial \ln w_e}{\partial\xi} + \frac{\partial \ln h_\phi}{\partial\xi} + \frac{\partial \ln u_e}{\partial\xi}\right] + \frac{h_\xi}{h_\phi}\left(G^2 - \textcircled{H}\right)\frac{1}{u_e}\frac{\partial w_e}{\partial\phi} - \frac{u_e}{h_\phi}\frac{1}{w_e}(h_\xi)_{\phi\phi}\right.$$

$$\left.\left(F^2 - \textcircled{H}\right)\right\} = \frac{\partial}{\partial\eta}\left(\tilde{\rho}\tilde{\mu}G_\eta\right) \qquad (12)$$

energy

$$V_2\textcircled{H}_\eta + \frac{2t}{\Lambda}F\textcircled{H}_\xi = \tilde{\rho}\tilde{\mu}M_e^2(\gamma-1)F_\eta^2 + \frac{1}{Pr}\frac{\partial}{\partial\eta}\left(\tilde{\rho}\tilde{\mu}\textcircled{H}_\eta\right)$$

$$+ \frac{2t}{\Lambda}\textcircled{H}\left(F - G\right)\left[\frac{\gamma-1}{\gamma}\frac{\partial P}{\partial\xi} + \frac{u_\infty}{u_e}M_e^2(\gamma-1)\left(\frac{u_e}{u_\infty}\right)_\xi\right]$$

where $G = W/w_e$

Near the stagnation point ($\xi = 0$), Taylor series expansions have been used for W_e, U_e, and h_ϕ,

$$W_e = a_1\xi + a_2\xi^2 + \cdots$$

$$U_e = b_1\xi + \cdots \qquad (13)$$

$$h = h\xi + \cdots$$

It should be noted that a distinction (31) must be made between the cases when $a_1 \neq 0$ and $a_1 = 0$. Eq. (11) can be further simplified to the following form at the stangation point,

continuity

$$(V_2)_\eta + F + \frac{h_\xi}{2h}\left[G\frac{a_1}{b_1} + G\frac{\partial}{\partial\phi}\left(\frac{a_1}{b_1}\right)\right] + G\frac{a_1}{b_1} = 0$$

ξ momentum

when $a_1 \neq 0$

$$V_2 G_\eta + FG - \textcircled{H} + \frac{h_\xi}{h}\frac{1}{2}\left(G^2 - \textcircled{H}\right)\frac{1}{b_1}\frac{\partial a_1}{\partial\phi} + \frac{h_\xi}{h}\frac{a_1}{b_1}GG_\phi = \frac{\partial}{\partial\eta}\left(\tilde{\rho}\tilde{\mu}G_\eta\right)$$

when $a_1 = 0$,

$$V_2 G_\eta + \frac{3}{2}\left(FG - \textcircled{H}\right) - \frac{3}{2}\left(F^2 - \textcircled{H}\right) = \frac{\partial}{\partial \eta}\left(\tilde{\rho}\tilde{\mu} G_\eta\right)$$

ξ momentum

$$V_2 F_\eta + \frac{1}{2} G \frac{a_1}{b_1}\frac{h_\xi}{h} F_\phi + \frac{1}{2}\left(F^2 - \textcircled{H}\right) + \frac{a_1}{2b_1}\left(FG - \textcircled{H}\right)\left[\frac{h_\xi}{b_1 h}\frac{\partial b_1}{\partial \phi} + \frac{1}{h}\frac{\partial h_\xi}{\partial \phi}\right] - \frac{1}{2}\left(\frac{a_1}{b_1}\right)^2\left(G - \textcircled{H}\right) = \frac{\partial}{\partial \eta}\left(\tilde{\rho}\tilde{\mu} F_\eta\right) \qquad (14)$$

energy:

$$V_2 \textcircled{H}_\eta + \frac{G}{2}\frac{a_1}{b_1}\frac{h_\xi}{h}\textcircled{H}_\phi = \frac{1}{Pr}\frac{\partial}{\partial \eta}\left(\tilde{\rho}\tilde{\mu}\textcircled{H}_\eta\right)$$

There is no restriction on the magnitude of w in eq. (11-14), therefore, the governing system is not limited to small cross-flow. Finally the boundary conditions for eqs. (11-14) are

$$\eta = 0\,, \quad F = W = V_2 = G = 0$$
$$\textcircled{H} = \textcircled{H}_w \quad \text{or} \quad \textcircled{H}_\eta = 0$$

$$\eta = \eta_e\,, \quad F = \textcircled{H} = G = 1$$
$$W = W_e/U_e$$

III.1.B Afterbody Supersonic Region

Downstream of the blunt nose, the formulation described in Ref. 30 is adopted here. The conventional boundary layer equations are modified to include all pertinent effects of cross flow diffusion and centrifugal force. With the usual boundary-layer approximations

$\frac{\partial}{\partial y} \gg \frac{\partial}{\partial x}$, Re$\gg$ 1 and the retention of cross-diffusion terms, required to adequately describe boundary regions or local shear flows formed near separation plane, the Navier-Stokes equations can be reduced to ,

continuity

$$x(\rho u)_x - \frac{\eta}{2}(\rho u)_\eta + (\rho v)_\eta + \frac{x}{r}\left[\sin\alpha(\rho w)_\phi + \rho u r_x\right.$$

x: momentum $\left. + \rho v\left(Re \cdot x\right)^{-\frac{1}{2}} r_y\right] = 0$

$$x\rho u u_x - \frac{\eta}{2}\rho u u_\eta + \rho v u_\eta + \frac{\rho w \sin\alpha}{r} x u_\phi - \frac{x}{r}\rho w^2 \sin^2\alpha\, r_x = -\frac{x}{M_\infty^2}\gamma P_x + \left(\mu u_\eta\right)_\eta + \sqrt{\frac{x}{Re}}\frac{\mu}{r} r_y u_\eta + \frac{x}{r^2}\frac{1}{Re}\left[\left(\mu u_\phi\right)_\phi\right]$$

y: momentum $P_\eta = M_\infty^2 \gamma \sin^2\alpha \sqrt{\frac{x}{Re}}\rho w^2 r_y r^{-1}$ (15)

ϕ momentum

$$x\rho u w_x - \frac{\eta}{2}\rho u w_\eta + \rho v w_\eta + \frac{\rho w \sin\alpha}{r} x w_\phi + \frac{\rho u w}{r} x r_x = -\frac{x}{M_\infty^2 \gamma r \sin\alpha} P_\phi + \left(\mu w_\eta\right)_\eta + \sqrt{\frac{x}{Re}}\frac{\mu}{r} r_y w_\eta + \frac{4}{3}\frac{x}{r^2}\frac{1}{Re}\left(\mu w_\phi\right)_\phi$$

energy

$$x\rho u T_x - \frac{\eta}{2}\rho u T_\eta + \rho v T_\eta + \frac{\rho w \sin\alpha}{r} x T_\phi + P(\gamma - 1) x\left[u_x - \frac{1}{2}\frac{\eta}{x} u_\eta + \frac{u r_x}{r} + \frac{\sin\alpha}{r} w_\phi\right.$$
$$\left. + \frac{v_\eta}{x} + \frac{v}{r} r_y \sqrt{\frac{1}{Re \cdot x}}\right] = \frac{\gamma}{Pr}\left[\left(\mu T_\eta\right)_\eta + \sqrt{\frac{x}{Re}}\frac{\mu}{r} r_y T_\eta\right] + M_\infty^2 \gamma(\gamma - 1)\mu\left[u_\eta^2 + \sin^2\alpha\, w_\eta^2\right] + \frac{1}{r^2}\frac{x}{Re}\left[\mu M_\infty^2 \gamma(\gamma - 1)\left(u_\phi^2 + \frac{4}{3}\sin^2\phi\, w_\phi^2 + \sin^2\alpha\, r_y w^2\right)\right.$$
$$\left. + \frac{x}{Pr}\left(\mu T_\phi\right)\phi\right]$$

The coordinate system is depicted in Fig. (1) and the governing system is not restricted to small cross flow. Here the boundary conditions for the boundary layer flow are:

$$\eta = 0\,, \quad u = v = w = 0\,, \quad T = T_w \quad T_\eta = 0$$

$$\eta = \eta_\delta\,, u = u_e\,, \quad w = w_e\,, \quad T = T_e$$

III.2 The Turbulence Model

In eqs. (11-15) it is postulated that the Reynolds stresses are related to the mean rate of strain via a turbulent eddy viscosity; i.e.

$\mu = \mu_\ell + \mu_t$, μ_ℓ = molecular viscosity

$$\mu_{t_1} = -\rho\overline{u'v'}/q_y\,, \mu_{t_2} = -\rho\overline{v'w'}/q_y \qquad (16)$$

A simple eddy viscosity model is based on Prandtl's mixing length hypothesis. For a three-dimensional boundary layer, it is assumed that μ_t is a scaler function independent of the coordinate direction. Accordingly, the eddy viscosity(32) can be written as:

$$\mu_t = \mu_{t_1} = \mu_{t_2} = \rho(\ell D)^2 q_y$$

where $q = (u^2 + w^2)^{1/2}$ (17)

$$\ell = \lambda\delta \tanh\left(\frac{0.41}{\lambda}\frac{y}{\delta}\right), \lambda = 0.09$$

D = Van Driest's damping function = $1 - \exp\left[-Y^+/A^+\right]$, $Y^+ = y\sqrt{\tau_w/\rho_w}/\nu_w$,

$A^+ = 26\sqrt{\rho_w/\rho}\left(\mu/\mu_w\right)$

For thick turbulent boundary layers with transverse curvature effects, Cebeci(33) has suggested the following modification in the wall region

$$\mu_t = \rho\frac{r}{r_w}\left\{0.41\, r_w \ell n\left(\frac{r}{r_w}\right)\left[1 - \exp\left(-\frac{r_w^+}{A^+}\ell n\frac{r}{r_w}\right)\right]\right\}^2 q_y$$

where

$$r_w^+ = r_w\sqrt{\tau_w/\rho}/\nu_w$$

Recently four independent experiments in different laboratories have found that the ratio $\alpha_1 = \mu_{t_2}/\mu_{t_1}$ is not unity as assumed in the isotropic model. In other words, the eddy viscosity is a tensor instead of an invariant scalar quantity. For example, Bissonnett and Mellor(34) are able to demonstrate that the eddy viscosity is a scalar only in

the small region near the wall, while α_1 decreases to an average value of 0.7 in the outer portion of the boundary layer. Three sets of independent European experimental measurements[35-37] have also suggested the value of α_1 can be as low as 0.4 through the outer region of the boundary layer.

Herein, the turbulence model will be modified to incorporate the nonistropic form; the magnitude of μ_t is dependent on the coordinate direction so that

$$\mu_{t_1} = \rho (l_1 D)^2 \, q_y \, , \quad \mu_{t_2} = \rho (l_2 D)^2 \, q_y \tag{18}$$

$$l_1 = \lambda_1 \delta \tanh \left(\frac{0.41}{\lambda_1} \frac{y}{\delta} \right)$$

$$l_2 = \lambda_2 \delta \tanh \left(\frac{0.41}{\lambda_2} \frac{y}{\delta} \right) \, , \quad \frac{\lambda_2}{\lambda_1} \leq 1$$

In this formulation, it has been shown that near the wall $l_1 = l_2 = 0.41\, y$, so that $\alpha_1 = 1$ is preserved; the two eddy viscosities will differ in the outer wake region.

In higher order theory, the eddy viscosity is assumed to be proportional to the transport properties. For example, in Jones and Launder's model, μ_t is determined by the local values of the density, turbulent kinetic energy k, and the dissipation function, ϵ. The governing differential equations for K and ϵ are:[38]

$$\rho \frac{DK}{Dt} = \frac{1}{r} \frac{\partial}{\partial r} \left[\left(\frac{\mu_\ell + \mu_t}{J_4} \right) r K_r \right] + \mu_t \left(u_y^2 + w_y^2 \right) - \rho \epsilon$$

$$\rho \frac{D\epsilon}{Dt} = \frac{1}{r} \frac{\partial}{\partial r} \left[\left(\frac{\mu_\ell + \mu_t}{J_5} \right) r \epsilon \right] + C_1 \frac{\epsilon}{K} \mu_t \left(u_y^2 + w_y^2 \right) - C_2 \rho \epsilon^2 / K \tag{19}$$

$$\mu_t = C_3 \rho K^2 \epsilon^{-1}, \quad C_1 = 1.45, \quad C_2 = 2\left(1 - 0.3 e^{-R_t^2}\right)$$

$$R_T = \frac{\rho K^2}{\mu_\ell \epsilon}$$

$$C_3 = 0.09 \exp \left| -2.5/\left(1 + R_t/50\right) \right|, J_4 = 1, \; J_5 = 1.3$$

This model contains five empirical constants which are determined from experimental data. The advantage of the k-ϵ model is that the flow history is taken into account. With some adjustment on the empirical constants, flow relaminarization or even transition can be considered.

The following boundary conditions are imposed on the equations for k and ϵ :

$$y = 0, \quad K = \epsilon = 0$$

$$y = \delta \, , \quad u_e \frac{\partial K}{\partial \xi} = -\epsilon \, , \; u_e \frac{\partial \epsilon}{\partial \xi} = -C_2 \frac{\epsilon^2}{K}$$

The turbulent thermal conductivity is assumed to take the following form:[38a]

$$K_t \, T_y = -\rho \overline{v' h'}$$

and

$$K_t = C_p \mu_t / Pr_t$$

$$Pr_t = 0.95 - 0.45 \, y/\delta$$

Finally, Dhawan and Narasimha's intermittency factor[39] is used to model the flow in the transitional region. The beginning of transition can be either specified in the (ξ, ϕ) plane or based on the $(Re_\theta) = f(M_{e_T})$ criterion.[46] For the present investigation, we are interested in evaluating the applicability of these simple closure models for the solution of three-dimensional boundary layer flows, including cases with cross flow reversal.

III.3 Numerical Methods

Numerical computations in blunt nose region are initiated at the stagnation point. A shooting method is used to integrate eq. (13). Then Krause's scheme[26] is employed to solve eq. (11) in a downstream marching fashion. The nonlinear terms in the finite difference equations are linearized by the Newton-Raphson procedure:

$$\begin{aligned} (UV)_L &= U_{L-1} V_L + U_L V_{L-1} - U_{L-1} V_{L-1} \\ (U_y^2)_L &= 2 (U_y)_L (U_y)_{L-1} - (U_y^2)_{L-1} \end{aligned} \tag{20}$$

where L denotes the iteration number.

The iteration continues until a specified convergence criteria is attained. The solution is obtained with an efficient "block tridiagonal" algoritem described in Reference (40).

A predictor-corrector scheme[27, 28] is used to continue the three dimensional boundary layer calculation into the supersonic afterbody region. Some modifications are made in the original P/C formulation in order to improve its efficiency and numerical stability restrictions. For turbulent flows, it has been found that a modified difference[41] representation for the lateral derivative $\partial(\,)/\partial\phi$, is superior to the standard central difference, i.e.

$$\left(\frac{\partial u}{\partial \phi} \right)_{M,K} = \frac{1}{\Delta \phi} \left| u_{M,K} - u_{M,K-1} \right| + \frac{\left| u_{M-1,K+1} + u_{M-1,K-1} - 2u_{M-1,K} \right|}{2\Delta\phi}$$

$$W > 0$$

$$= \frac{1}{\Delta \phi} \left| u_{M,K+1} - u_{M,K} \right| - \frac{\left| u_{M-1,K+1} + u_{M-1,K-1} - 2u_{M-1,K} \right|}{2\Delta\phi} \, , \quad W < 0 \tag{21}$$

where M and K denotes the indices in the ξ and ϕ direction respectively.

This procedure will result in a matrix system which is always diagonally dominant. Furthermore, it eliminates

wiggles which sometimes appear near the cross flow separation line. At the same time, the numerical accuracy of this method remains of second order.

In most cases, calculations were initiated at the windward plane. With the formulation given in eq. (21), a linear stability analysis shows that the P/C scheme is unconditionally stable for $w > 0$, with a CFL condition on the cross flow velocity w required if $w < 0$.

Because of the various length scales appearing in the turbulent flow (e.g. the laminar sublayer, wall and wake region), it is usually necessary to impose a coordinate transformation or to adopt a variable grid system. A simple mapping of the following form will serve this purpose:

$$Y = \ln \eta \quad \text{or} \quad Y = \eta^{\frac{1}{m}} \quad , \quad m \geq 2$$

When a variable mesh system is used, the conventional three-point finite difference quotient can be written as:

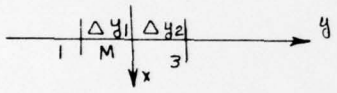

$$\left(\frac{\partial u}{\partial y}\right)_M = Z_a(J)\,u_3 + Z_b(J)\,u_M + Z_c(J)\,u_1 - \frac{\Delta y_1 \Delta y_2}{6}\frac{\partial^3 u}{\partial y^3} \qquad (22)$$

$$\left(\frac{\partial^2 u}{\partial y^2}\right)_M = Z_e(J)\,u_3 + Z_f(J)\,u_M + Z_g(J)\,u_1 + \frac{1}{3}\frac{\partial^3 u}{\partial y^3}(\Delta y_1 - \Delta y_2) + O(\Delta y^2)$$

where

$$Z_a(J) = \Delta y_1 / \left[\Delta y_2 (\Delta y_1 + \Delta y_2)\right]$$

$$Z_b(J) = (\Delta y_2 - \Delta y_1)/\Delta y_1 \Delta y_2$$

$$Z_c(J) = -\Delta y_2 / \left[\Delta y_1 (\Delta_1 + \Delta y_2)\right]$$

$$Z_e(J) = 2 / \left[\Delta y_2 (\Delta y_1 + \Delta y_2)\right]$$

$$Z_f(J) = -2/\Delta y_1 \Delta y_2$$

$$Z_g(J) = 2 / \left[\Delta y_1 (\Delta y_1 + \Delta y_2)\right]$$

The truncation error for U_{yy} is $O(\Delta y^2)$ when uniform grid is specified, but degenerates to $O(\Delta y_1 - \Delta y_2)$ with a variable mesh. It should be noted that U_y is always second order even for non-uniform grids.

In order to reduce the truncation error, one can evaluate U_{yyy} from the governing equations and substitute the resulting expression into the difference quotient, eq. (22). In doing so, a second order accurate system is obtained for U_{yy}. To illustrate this point, consider the simplified X - momentum equation near the wall,

$$B_1 = (\mu u_y)_y \qquad (22a)$$

One can estimate U_{yyy} by differentiating eq. (22a) and substituting into eq. (22). The result is

$$u_{yy} = \frac{Z_e(J)\,u_3 + Z_f(J)\,u_M + Z_g(J)\,u_1 - \frac{2}{3}(\Delta y_1 - \Delta y_2)\frac{\mu_y u_y}{\mu}}{1 + \frac{2}{3}\frac{\mu_y}{\mu}(\Delta y_1 - \Delta y_2)} + O(\Delta y^2) \qquad (23)$$

Here the term μ_{yy} is replaced by a first order relation, i.e.

$$\mu_{yy} = Z_e(J)\,\mu_3 + Z_f(J)\,\mu_M + Z_g(J)\,\mu_1 + O(\Delta y_1 - \Delta y_2) \qquad (23a)$$

Eq. (23a) results in a second order accurate representation for U_{yy}. Most of the results presented here are obtained with this type of formulation.

An alternating direction implicit method[44] which is unconditionally stable for linear systems was also examined. However, satisfactory results were obtained only for laminar flows.

III.4 Results for Three-Dimensional Viscous Flow Calculations

Figures (6) and (7) depict the heat transfer distribution on pointed[47] and blunt cones.[46] Laminar and turbulent flows have been studied and comparisons with experimental data are encouraging. The flow properties at the leeward plane of a sharp cone at large angle of attack are also predicted reasonably well (Fig. 6).

The Nusselt number distribution on a cone-cylinder-flare configuration[18] is shown in Fig. (8). Significantly, the calculations do predict the laminar heating overshoot in a region where a strongly favorable pressure gradient exists. It is noted that when the flow undergoes a rapid expansion (e.g. at the junction of cone and cylinder), the solution is very sensitive to the outer boundary conditions. The boundary layer thickness charges rapidly and it is no longer adequate to impose the condition $U \to U_e$ as $y \to \delta$. An alternate procedure suggested by Ackerberg and Philip[42] proves to be satisfactory. They use the fact that the velocity profiles[43] exhibit the following variation* for $\eta \gg 1$

$$u = u_e + a\eta^k \exp\left|-(\eta - b)^2/\Lambda_1\right| \qquad (24)$$

$$\Lambda_1 = \frac{4}{\xi^2}\int_0^{\xi} u_e\, d\xi$$

*Similar expressions can be written for the temperature.

where a, b and k are constant at fixed ξ. These values are determined by fitting eq. (24) to the velocity profile at the outer edge of the boundary layer. This procedure is incorporated into the implicit algorithm described previously.

The numerical results for the velocity and temperature profiles on a sharp cone are given on Fig. (9). The body geometry and free stream values correspond to Rainbird's experimental conditions.(48) When the eddy viscosity is treated as an invariant scalar (i.e eq. (17)), agreement between the numerical prediction and Rainbird's data is good for $\phi \leq 135^{\circ}$ (Fig. 9). But the comparison deteriorates somewhat as the leeward plane is approached. Similar observations apply for the limiting streamline inclination (Fig. 10). It is significant that the Prandtl mixing length theory, with a scalar eddy viscosity implies an attached boundary layer; the experimental measurements indicate that cross flow separation occurs for $\phi > 160^{\circ}$. To the authors' knowledge, this is the first time that theoretical results have been reported for the turbulent flow near the leeward plane where secondary flow reversal has occurred.

The calculated windward plane results using the two-equation model for Reynolds stress closure are also shown on Fig. 9a. The agreement with the data is good. There is no apparent advantage in using this higher order theory, since the simple modified mixing length model leads to an equally accurate prediction at the windward plane. At the present time numerical computations using the two-equation model have been made only at the symmetry plane.

In order to improve the comparison between the numerical results and the experimental data near the leeplane, some modifications of the eddy viscosity formulations are required. As discussed previously, experimental measurements(34-37) suggest that the eddy viscosity is not an isotropic scalar quantity in the outer wake region. Although the distribution of μ_{t_1} and μ_{t_2} across the boundary layer cannot be measured accurately at the present time, the mean value of the ratio $\alpha_1 = \mu_{t2}/\mu_{t1}$ has been found to be as large as 0.7 (Ref. 33) and as low as 0.4 (Ref. 34, 36, 37). Fig. (10) shows the numerical results for the surface limiting streamline inclination for nonisotropic eddy viscosity distributions as given in eq. (18). For this calculation $\lambda_1 = 0.09$, $\lambda_2 = 0.064$ and $\alpha_1 = 0.5$ are assumed. For $\phi > 160^{\circ}$, there does not appear to be any significant improvement over the isotropic model.

Bradshaw,(53) Baker and Jones(54) have pointed out that the mixing length theory may become inadequate to predict the flows in which the boundary layer thickness grows rapidly (such as flow under adverse pressure gradients). In this case, because of the convective transport of turbulence, the magnitude of the mixing length in the outer part of the boundary layer does not increase as fast as the boundary layer thickness. In other words, the eddies which may have originated near the windward plane, carry some of the character of the boundary layer at an earlier stage of its development. Near the leeplane a rapid thickening of the boundary layer occurs. The mixing length is in fact indicative of the flow some distance upstream, where δ was appreciably thinner. Consequently, the apparent value of λ_1 in eqs. (17) or (18) falls. Here an adjustment for this effect is made by reducing the constant λ_1 from 0.09 to 0.063 for the flow near the leeward plane ($\phi \geq 145^{\circ}$). Results are given on Figs. (9E) and (10). Crossflow separation is predicted somewhat more accurately with this modification, although the improvement is only marginal.

IV. The Coupled Viscous and Inviscid Flow Computations

Solutions for the inner and outer layers are now coupled in order to take into account the viscous-inviscid interaction. For the inviscid (outer) flow computations, the viscous displacement(50) is included by considering the effective body shape as modified by

$$r_{eff}(z,\phi) = r_w(z,\phi) + \Delta \cos\theta \qquad (25)$$

Δ is the three dimensional displacement thickness, which must be obtained from the partial differential equation:

$$\frac{\partial}{\partial x}\left[\rho_e u_e r(\Delta - \delta_x^*)\right] + \frac{\partial}{\partial \phi}\left[\rho_e w_e(\Delta - \delta_\phi^*)\right] = 0 \qquad (26)$$

where $\delta_\phi^* = \int_0^\delta (1 - \rho w/\rho_e w_e)\, dy$

$$\delta_x^* = \int_0^\delta (1 - \rho u/\rho_e u_e)\, dy$$

The body entropy value, S_w (x), is estimated by the steamtube replacement at the windward plane, i.e.

$$r_s^2 = 2\frac{\rho_e u_e}{\rho_\infty u_\infty} r_w \Delta, \quad S_w = S_s(r_s, 0)$$

The procedure for evaluating S_w is demonstrated in Fig. 1. Our formulation bypasses the thin "entropy or vortical layer" effect which can lead to numerical instability when $Z/R_N \gg 1$.

For the inner layer computations,

the boundary layer edge properties are obtained by interpolating the inviscid properties at $r_w = r_w + d\cos\theta$. Here d is found from(49)

$$d = \delta - \Delta \tag{27}$$

When the external inviscid flow is highly rotational, then the following criterion(49a, 51) is used to define the local value of δ,

$$\left(h + \frac{q^2}{2} - h_w\right)\Big/\left(H_o - h_w\right) = 0.99 \tag{28}$$

This condition replaces the conventional procedure of setting $U_y = T_y = 0$ as $y \to \infty$. However, for adiabatic walls it is necessary to revert to the conventional $U_y = 0$ condition to locate the boundary layer edge. This implies that the inner flow calculation contains part of the inviscid vortical layer.

The procedure for the numerical computation starts with the calculation of the outer flow. The inviscid information is input into the inner layer calculations. However, when the Euler equations are integrated at $z = z_1$, the local value of Δ is still unknown as the boundary layer calculations have not reached z_1. Herein, a "cyclic iteration" procedure is employed. We initiate the calculations of the outer layer by estimating two sets of values $\partial\Delta/\partial x$. These are obtained from Taylor series extrapolations:

$$\psi_a^{(1)} = 2\left(\frac{\partial\Delta}{\partial x}\right)_M - \left(\frac{\partial\Delta}{\partial x}\right)_{M-1}$$

$$\psi_a^{(2)} = \psi_a^{(1)} + 0.5^\circ$$

and $$\Delta_{M+1} = \Delta_M + \left(\frac{\partial\Delta}{\partial x}\right)\Delta x$$

After completing the inviscid flow computations, this information is input to the three dimensional boundary layer computations from which corrected values of $\psi_c = (\partial\Delta/\partial x)_{M+1}$ are obtained. Then a new estimate for $\partial\Delta/\partial x$ is written as(55, 56)

$$\frac{\partial\Delta}{\partial x} = \frac{\psi_a^{(1)}\psi_c^{(2)} - \psi_c^{(1)}\psi_a^{(2)}}{\psi_c^{(2)} - \psi_c^{(1)} + \psi_a^{(1)} - \psi_a^{(2)}} \tag{29}$$

The iteration procedure continues until convergence is achieved. During the development of the numerical program it was found that a fixed-point iteration (i.e. using the most recently calculated $\partial\Delta/\partial x$ for the next cycle of calculation) converges quite slowly for certain flow conditions and, therefore, becomes impractical. However, a Newton-Raphson procedure (i.e. eq. (29)) works satisfactorily in all cases tested so far. Usually 3 iterations are necessary.

The numerical procedures of coupling the inner and outer flow have been applied to a number of test cases; however, for the present paper only one case will be presented. Sample results considered here are for the supersonic flow over a sphere-cone ($\theta = 9^\circ$) at 10° angle of attack. Free-stream flow properties are based on Widhopf's(46) experimental conditions. The inviscid blunt body results are obtained by the time dependent method without the viscous displacement correction, since this effect is small in the blunt nose region for the high Reynolds number flow ($Re_\infty = 1.8 \times 10^7$/ft., $M_\infty = 5$) studied here. The Blottner and Ellis formulation is used for the inner boundary layer calculations which are initiated at the stagnation point.

In the supersonic conical section the inner and outer flows are determined by a marching procedure. Viscous displacement and entropy swallowing are included in the iterative matching of the two regions. A three-point Lagrange's formula is used to interpolate the boundary layer edge conditions from the inviscid flow properties.

The surface coordinates for the blunt body boundary layer calculations are illustrated in Fig. (11). The heat transfer distribution on the body is depicted in Fig. (12). Here the transition points are specified from the experimental measurements. It is shown in Fig. 12 that the heating (for $z/R_N \leq 5$) will be underpredicted by at most 5% when entropy layer swallowing effects are not included. These effects will become more important at higher Mach numbers and lower Reynolds number. It is also found that the viscous displacement effects have a small influence on the inviscid pressure distribution for the flow conditions under investigations (Fig. 13). Perhaps this is expected since Δ/r_w is always less than 0.1. Comparisons between the numerical results and Widhopf's data (heat transfer and surface pressure) is good.

V. Summary

A method has been developed for treating the viscous flow over a blunt or sharp body at angle of attack. Herein, a two layer model is suggested. The inner region consists of the three dimensional boundary layer and boundary region. Laminar and turbulent flows are considered. The governing system can handle problems with cross flow reversal and is integrated by predictor-

corrector or alternating direction implicit method. The outer inviscid flow is computed with MacCormack's two level finite difference scheme, with the bow shocks treated as discontinuities. The salient features for matching these two regions include the effects of the three dimensional viscous displacement and entropy layer swallowing. It is only necessary to input the body geometry, free-stream flow properties and the surface conditions. The numerical results include the aerodynamic coefficients, heat transfer and the detailed flow profiles.

The general treatment of the problem and the method of solution are verified by the good agreement obtained between results from the present formulation and the experimental data. It is observed in our preliminary results that: (1) the simple scalar mixing length theory for the Reynolds stress exhibits minor defects in regions with cross flow separation. Some adjustments are necessary in order to obtain a better comparison with experimental data; (2) for numerical results not shown here, the viscous displacement effects may become more pronounced in laminar than turbulent flow and (3) the entropy-layer swallowing is of only minor importance for the examples considered here; nevertheless, it is expected that this phenomena can become dominant at hypersonic speeds and for low Reynolds numbers.

Work in progress includes the following investigations: (i) supersonic flow over cones at large angles of attack ($\alpha/\theta \geq 1.5$; attention will focus on the existence of inviscid solutions), (ii) optimization of the numerical procedures for coupling the inner and outer flow and for the interpolation of the boundary layer edge properties, and (iii) the application of improved Reynolds stress modelling for the three-dimensional boundary layer.

VI References

1. Blottner, F. G., "Finite Difference Methods of Solution of the Boundary Layer Equations," AIAA J., Vol. 8, No. 2, Feb. 1970, pp. 193-205.

2. Keller, H. B. and T. Cebeci, "Accurate Numerical Methods for Boundary Layer Flows. Part I. Two-Dimensional Laminar Flows," Lecture Notes in Physics, No. 8, Springer-Verlag, N. Y. 1971, pp. 92-100.

3. Barttlet, E. P. and R. M. Kendall, "Non-similar Solution of the Multicomponent Laminar Boundary Layer by an Integer Matrix Method," NASA CR-1062, March 1967.

4. Moretti, G. and Bleich, G., "Three-Dimensional Flow around Blunt Bodies," AIAA, J., Vol. 5, pp. 1557-1562, 1967.

4a. Moretti, G., Grossman, B. and Marconi, F., "A Complete Numerical Technique for the Calculation of Three-Dimensional Inviscid Supersonic Flows," AIAA paper 72-192, 1972.

5. Boger, R.C., "Three Dimensional Inviscid Flow Field Analysis of Aerodynamic Trim," AVSD-0272-73-RR, Aug. 1973.

6. Kutler, P., Reinhardt, W.A. and Warming, R.F., "Numerical Computation of Multishocked, Three Dimensional Supersonic Flow Fields with Real Gas Effects," AIAA paper 72-702, 1972

7. Inouye, M., Rakish, J.V., and Lomax, H., "A Description of Numerical Methods and Computer Programs for Two-Dimensional and Axisymmetric Supersonic Flow over Blunt Nosed and Flare Bodies," NASA TND-2970, August 1965.

8. Cheng, S.I., "Numerical Intergration of Navier-Stokes Equations," AIAA J., 8, 12, pp. 2115-2122, Dec. 1970.

9. Baldwin, B.S. and MacCormack, R.W., "Numerical Solution of the Interaction of a Strong Shock Wave with a Hypersonic Turbulent Boundary Layer," AIAA paper No. 74-558, June 1974.

10. Luband, S.C. and Helliwell, W.S., "Calculation of the Flow on a Cone at High Angle of Attack," AIAA J., Vol. 12, pp. 965-974, July 1974.

11. Davis, R.T., "Numerical Solution of Hypersonic Viscous Shock-Layer Equations," AIAAJ., Vol. 8, pp. 845-851, May 1970.

12. Rubin, S.C., Lin, T.C., Pierucci, M., and Rodman, S., "Hypersonic Interaction along a Rectangular Corner," AIAA J., pp. 2241-2246, Nov. 1969.

13. Lubard, S.C. and Rakish, J., "Calculation of the Flow on a Blunted Cone at High Angle of Attack," AIAA paper 75-149 (1975).

14. Pandolfi, M., "Numerical Analysis of the Supersonic Flow about Elliptical Cones," Publicazione No. 157, Instituto Di Machine E. Motori Per Aeromobil, Torino, Italy, Feb. 1974.

15. Moretti, G. and Pandolfi, M., "Analysis of the Inviscid Flow about a Yawed Cone, Preliminary Studies," PIBAL Report 72-18, 1972.

16. MacCormack, R.W., "An Introduction to Numerical Solution of the Navier-

Stokes Equations," AIAA paper 75-1, AIAA 13th Aerospace Sciences Meeting, January 1975.

17. Zakkay, V. and Visich, M., Jr., "Experimental Pressure Distribution on Conical Elliptical Bodies at M_{∞} = 3.09 and 6," PIBAL Report No. 467, 1959.

18. Zakkay, V. and Callahan, C.J., "Laminar, Transition and Turbulent Heat Transfer to a Cone-Cylinder-Flare Body at Mach 8," J. Aero. Sci., pp. 1403-1413, December 1962.

19. Adams, J.C., "Analysis of the Three-Dimensional Compressible Turbulent Boundary Layer on a Sharp Cone at Incidence in Supersonic and Hypersonic Flow," AEDC-TR-72-66, June 1972.

20. Cebeci, T., "Attachment-Line Flow on an Infinite Swept Wing," AIAA J., Vol. 12, 1974, pp. 242-245.

21. Fannelop, T.K., and Humphreys, D., "A Simple Finite Difference Method for Solving the Three Dimensional Turbulent Boundary-Layer Equations," AIAA paper 74-13 (1974).

22. Der, J., "A Study of General Three-Dimensional Boundary Layer Problems by an Exact Numerical Method," AIAA J. Vol. 9, No. 7, pp. 1294-1302 (1971).

23. Popinski, Z. and Davis, R. T., "Three Dimensional Compressible Laminar Boundary Layer on Sharp and Blunt Circular Cones at Angle of Attack," NASA CR-112316, January 1973.

24. Harris, J.E., and Morris, D.J., "Solution of the Three Dimensional Compressible Laminar and Turbulent Boundary Layer Equations with Comparison to Experimental Data," paper presented at the Fourth International Conference on Numerical Method in Fluid Dynamics, Boulder, Colorado, June, 1974.

25. Dwyer, H.A., "Solution of a Three-Dimensional Boundary Layer Flow with Separation," AIAA J., pp. 1336-1342, July 1968.

26. Krause, E., "Comment on Solution of a Three-Dimensional Boundary Layer Flow with Separation," AIAA J., Vol. 7, No. 3 (1969).

27. Rubin, S.G. and Lin, T.C., "A Numerical Method for Three-Dimensional Viscous Flow: Application to the Hypersonic Leading Edge," J. Comp. Phys., Vol. 9, No. 2, April 2, pp. 339-364.

28. Rubin, S. G., "A Predictor-Corrector Method for Three Coordinate Viscous Flows," paper presented at the International Numerical Computation in Fluid Mechanics, held at Paris, France, 1972.

29. Lin, T.C. and Rubin, S.G., "Viscous Flow over a Cone at Moderate Incidence, I. Hypersonic Tip Region," Int. J. Computer and Fluids, Vol. I, pp. 37, 1972.

30. Lin, T.C. and Rubin, S.G., "Viscous Flow over a Cone at Incidence, II. Supersonic Boundary Layer," J. Fluid Mech., Vol. 59, July 1973, pp. 593-620.

30a. Rubin, S.G., Lin, T.C. and Tarulli, F. "The Viscous Layer in the Symmetry Plane of a Sharp Cone at Incidence," Polytechnic Institute of New York Report (to appear).

31. Blottner, F.G. and Ellis, M.A., "Three Dimensional Incompressible Boundary Layer on Blunt Bodies," Sandia Laboratory, SLA-73-0366, February 1973.

32. Hunt, J.L. Bushnell, D.M. and Beckwith, I.E., "The Compressible Turbulent Boundary Layer on a Blunt Swept Slab with or Without Leading Edge Blowing," NASA-SP-228, pp. 417-472, 1968.

32a. Shang, J.S., Hankey, J. and Dwoyer, D.L., "Numerical Analysis of Eddy Viscosity Model in Supersonic Turbulent Boundary Layer, AIAA J., 11, pp. 1677-1683, Dec. 1973.

33. Cebeci, T., "Eddy-Viscosity Distribution in Thick Axisymmetric Turbulent Boundary Layers," J. Fluids Engineering, pp. 319-326, June 1973.

34. Bissonnette L.R. and Mellor, G., "Experiments on the Behavior of an Axisymmetric Turbulent Boundary Layer with a Sudden Circumferential Strain," J. Fluid Mech. Vol. 63, pp. 369-413 (1974).

35. Vermeulen, A.J., "Measurements of Three-Dimensional Turbulent Boundary Layers," Ph.d. Thesis, U. of Cambridge, 1971.

36. East, L.F., "Measurements of the Turbulent Boundary Layers on a Slender Wing," paper presented at Euromech 33, Berlin 1972.

37. Van den Berg, B. and Elsenaar, A., NLR report to be published.

38. Jones, W.P. and Launder, B.E., "The Calculation of Low Reynolds Number Phenomena with a Two Equations Model of Turbulence," Int. J. Heat Mass Transfer, Vol. 16, pp. 1119-1130, 1973.

38a. Rotta, J., "Turbulent Boundary Layer in Incompressible Flow," Progress in Aero. Sci., Vol. 2, 1962.

39. Dhawan, S. and Narasimna, R., "Some Properties of Boundary Layer Flow during Transition from Laminar to Turbulent Motion," J. Fluid Mech., Vol. 13, June 1958, pp. 418-436.

40. Reyhner, T.A. and Flugge-Lotz, I., "The Interaction of a Shock Wave with a Laminar Boundary Layer," Ph.D. Thesis, Standord University, 1967.

41. Khosla, P.K. and Rubin, S.G., "A Diagonally Dominant Second-Order Accurate Implicit Scheme," J. Computers and Fluids, Vol. 2, pp. 207-209 (1974).

42. Ackerberg, R.C. and Phillips, J.H., "A Numerical Method for Highly Accelerated Laminar Boundary-Layer Flows," SIAM J. Numer. Anal., Vol. 10, No. 1, March 1973.

43. Brown, S.N. and Stewartson, K., "On Similarity Solutions of the Boundary-Layer Equations with Algebraic Decay," J. Fluid Mech. 23, (1965) pp. 673-687.

44. Nardo, C.T. and Cresci, R.J., "Merged Layer Flow Over a Finite Width Plate," AIAA paper 70-784, June 1970.

45. Polek, T.E. and Mateor, "Measurement of Turbulent Heat Transfer of Cones and Swept Plates at Angle of Attack," NASA-SP-216, pp. 455-472, December 1968.

46. Widhopf, G.F., "Laminar, Transitional and Turbulent Heat Transfer Measurement on a Yawed Blunt Conical Nosetip," SAMSO-TR-72-209, Sept. 1972.

47. Cresci, R.J. and Brodie, J., Private Communication.

48. Rainbird, W.R., "Turbulent Boundary Layer Growth and Separation on a Yawed Cone," AIAA J., Vol. 6, No. 12, pp. 2140-2146, December 1968.

49. Mayne, A.W., "Analysis of Laminar Boundary Layer on Right Circular Cones at Angle of Attack, Including Streamline Swallowing Effects," "AEDC-TR-72-134, October 1972.

49a. Mayne, A.W. and Adams, J.C., "Streamline Swallowing by Laminar Boundary Layer in Hypersonic Flow," AEDC-TR-71-32, March 1971.

50. Fannelop, T.K. and Waldman, G. D., "Displacement Interaction and Flow Separation on Cones at Incidence to a Hypersonic Stream," paper presented at AGARD, London, England, May 1968.

51. Levine, J.N. "Finite Difference Solution of the Laminar Boundary Layer in Hypersonic Flow," AEDC-TR-71-32, March 1971.

52. Stetson, K.F., "Boundary-Layer Separation on Slender Cones at Angle of Attack," AIAA J., Vol. 10, No. 5, May 1972, pp. 642-648.

53. Bradshaw, P., "The Response of a Constant-Pressure Turbulent Boundary Layer to the Sudden Application of an Adverse Pressure Gradient," ARC RM No. 3575 (1969).

54. Baker, R.J. and Launder, B.E., "The Turbulent Boundary Layer with Foreign Gas Injection--II. Predictions and Measurements in Severe Streamwise Pressure Gradients," Int. J. Heat Mass Transfer, Vol. 17, pp. 293-306, 1974.

55. Blottner, F.G. and Flugge-Lotz, I., "Finite-Difference Computation of the Boundary Layer With Displacement Thickness Interaction," Journal de Mecanique, Vol. II, No. 4, 1963.

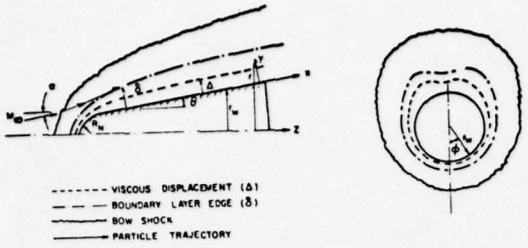

Fig. 1 Formulation and Notation

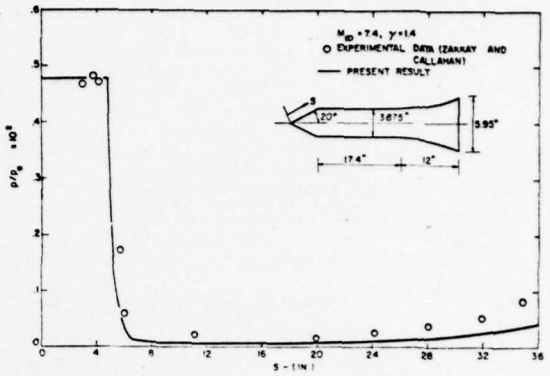

Fig. 4 Pressure Distribution on Cone-Cylinder-Flare

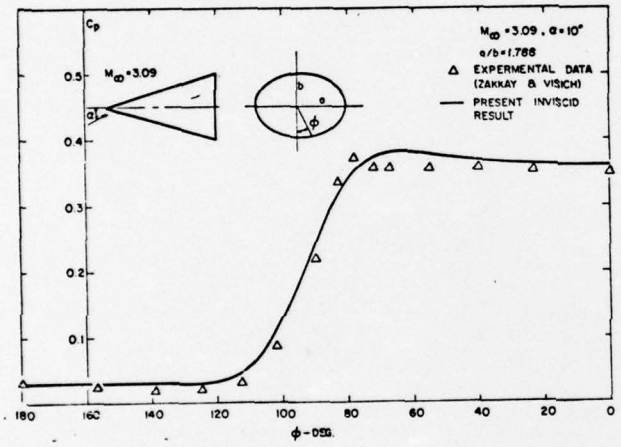

Fig. 2 Pressure Distribution on Elliptic Cone

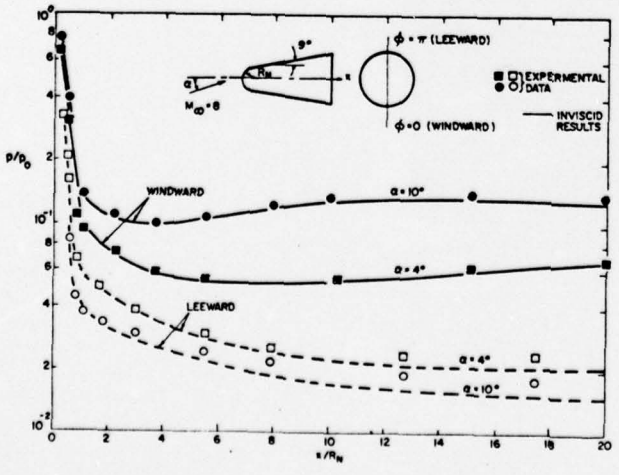

Fig. 3 Surface Pressure Distribution on Sphere-Cone

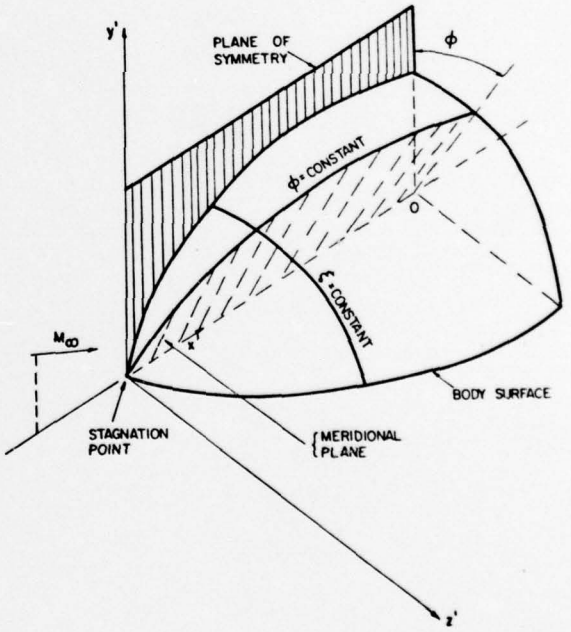

Fig. 5 Blunt Body: Surface Coordinate System

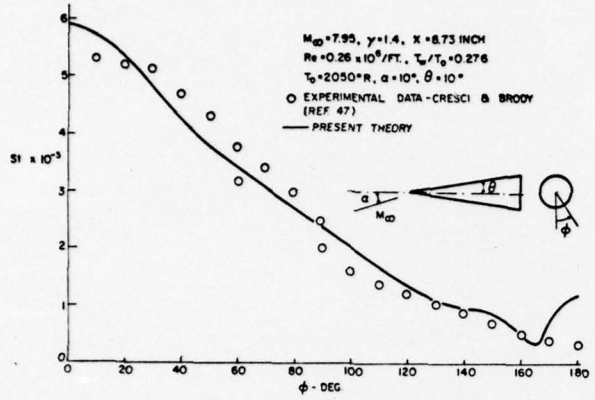

Fig. 6a Laminar Heat Transfer Distribution on a Pointed Cone at Angle of Attack

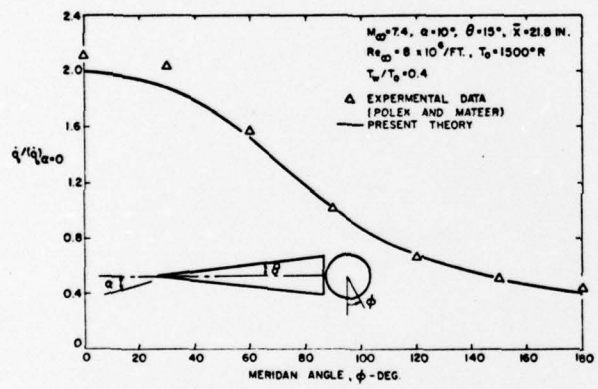

Fig. 6b Turbulent Heat Transfer Distribution on a Pointed Cone at Angle of Incidence

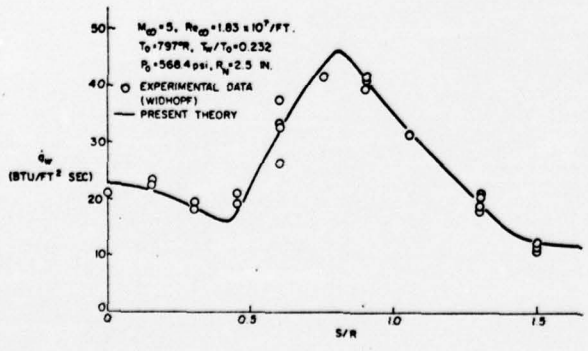

Fig. 7 Heat Transfer Distribution on Blunt Cone

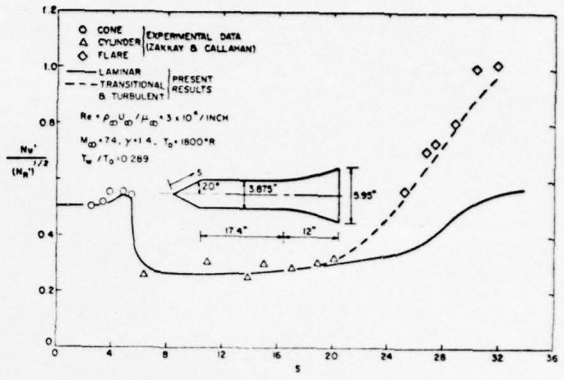

Fig. 8 Heat Transfer on Cone-Cylinder-Flare

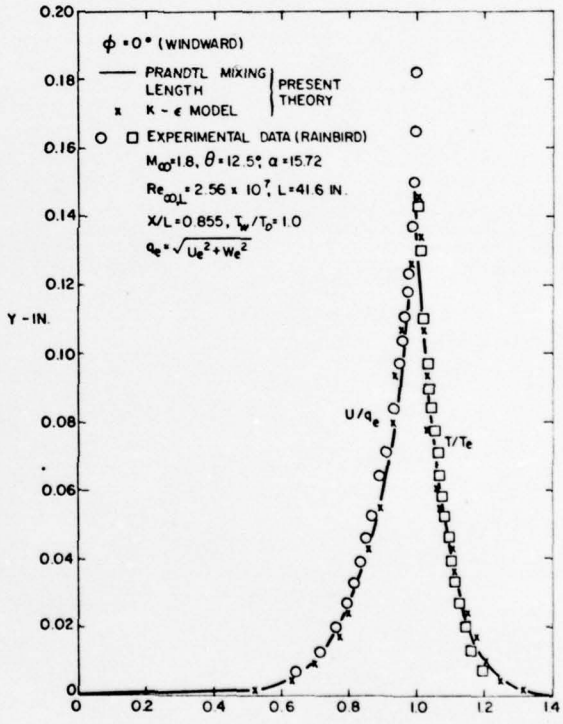

Fig. 9a Flow Profiles on a Pointed Cone

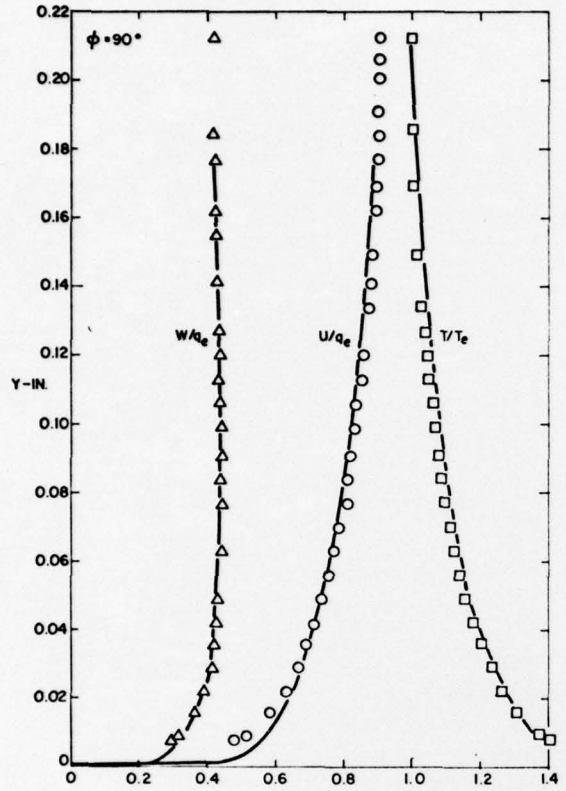

Fig. 9b Flow Profiles on a Pointed Cone

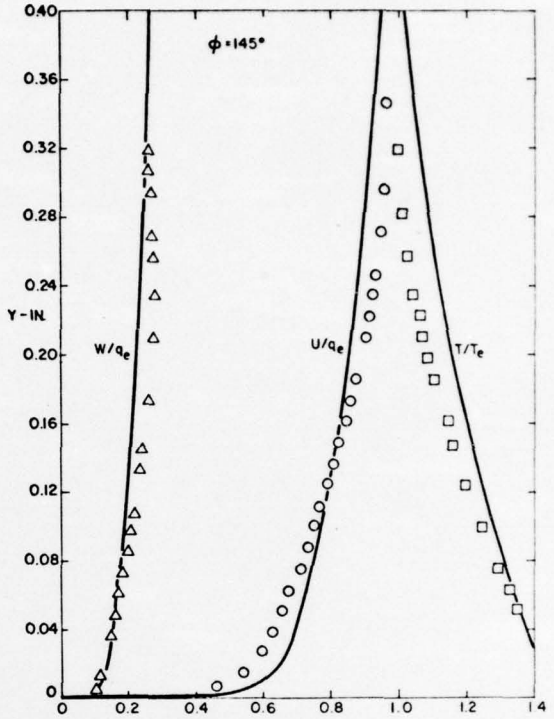

Fig. 9d Flow Profiles on a Pointed Cone

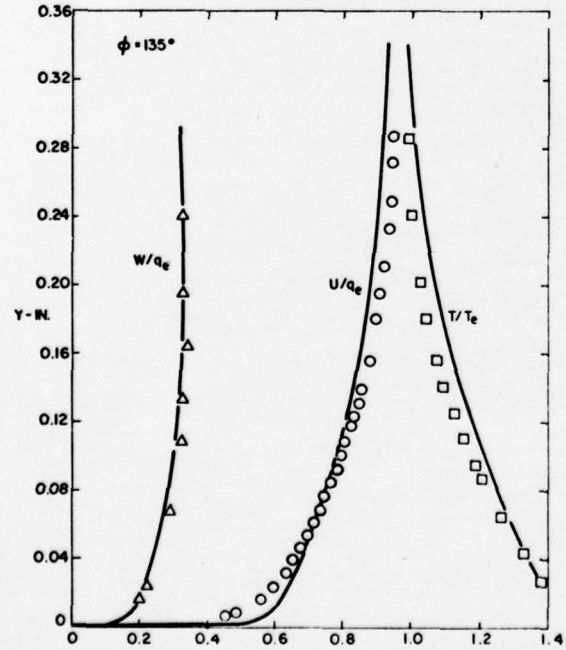

Fig. 9c Flow Profiles on a Pointed Cone

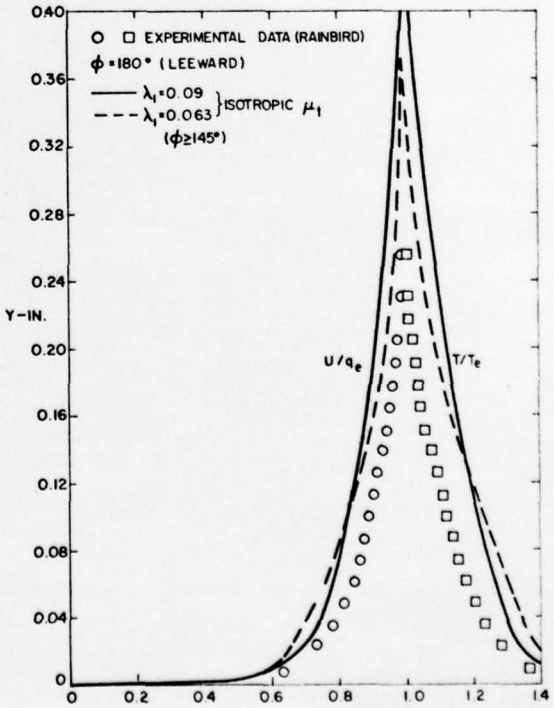

Fig. 9e Flow Profiles on a Pointed Cone

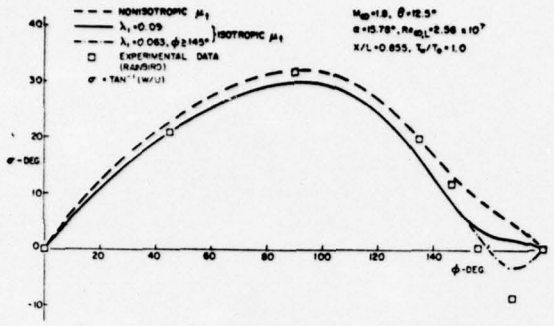

Fig. 10 Surface Limiting Streamline Inclination

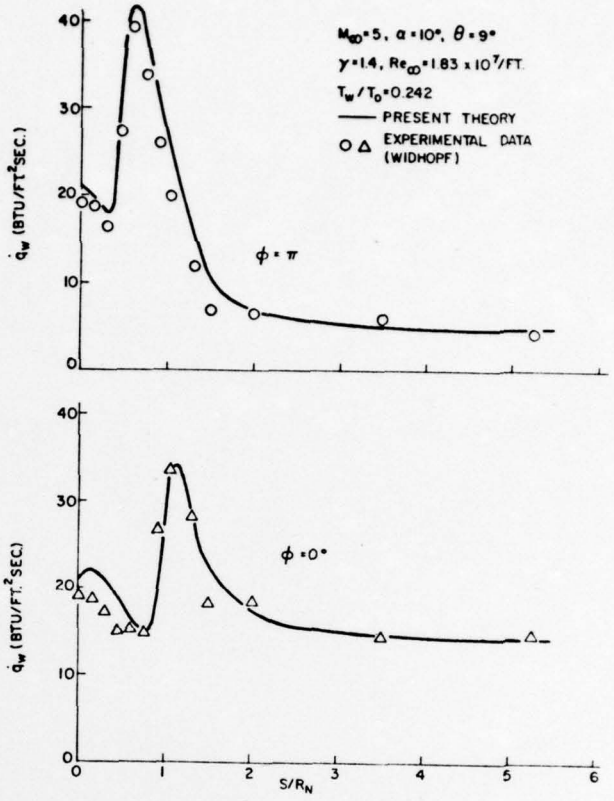

Fig. 12a Heat Transfer Distribution on Sphere-Cone at 10° Angle of Attack

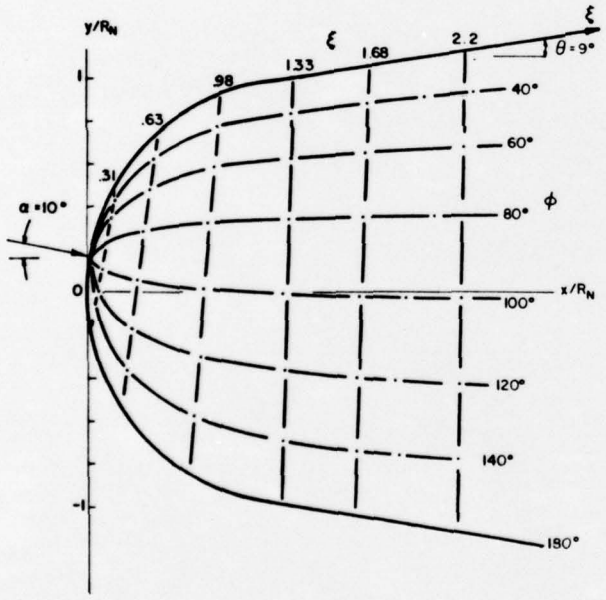

Fig. 11 Surface Coordinate on Sphere-Cone at 10° Angle of Incidence

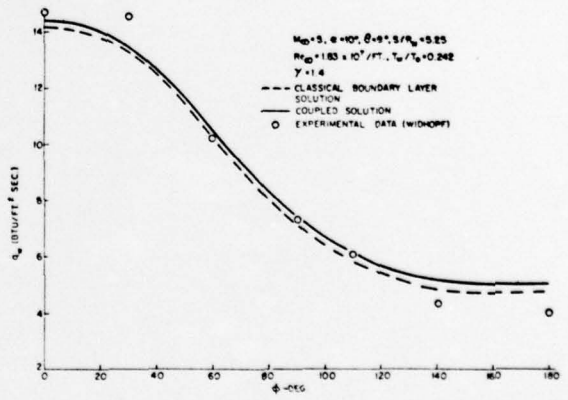

Fig. 12b Heat Transfer Distribiton on Sphere-Cone at 10° Angle of Attack

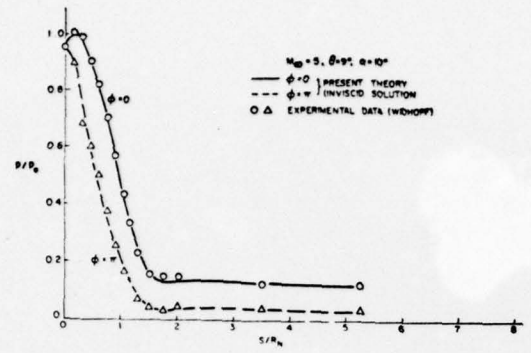

Fig. 13a Surface Pressure Distribution on Sphere-Cone at 10^0 Angle of Attack

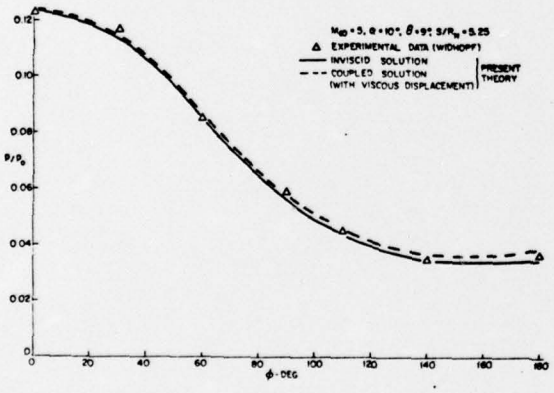

Fig. 13b Surface Pressure Distribution on Sphere-Cone at 10^0 Angle of Attack